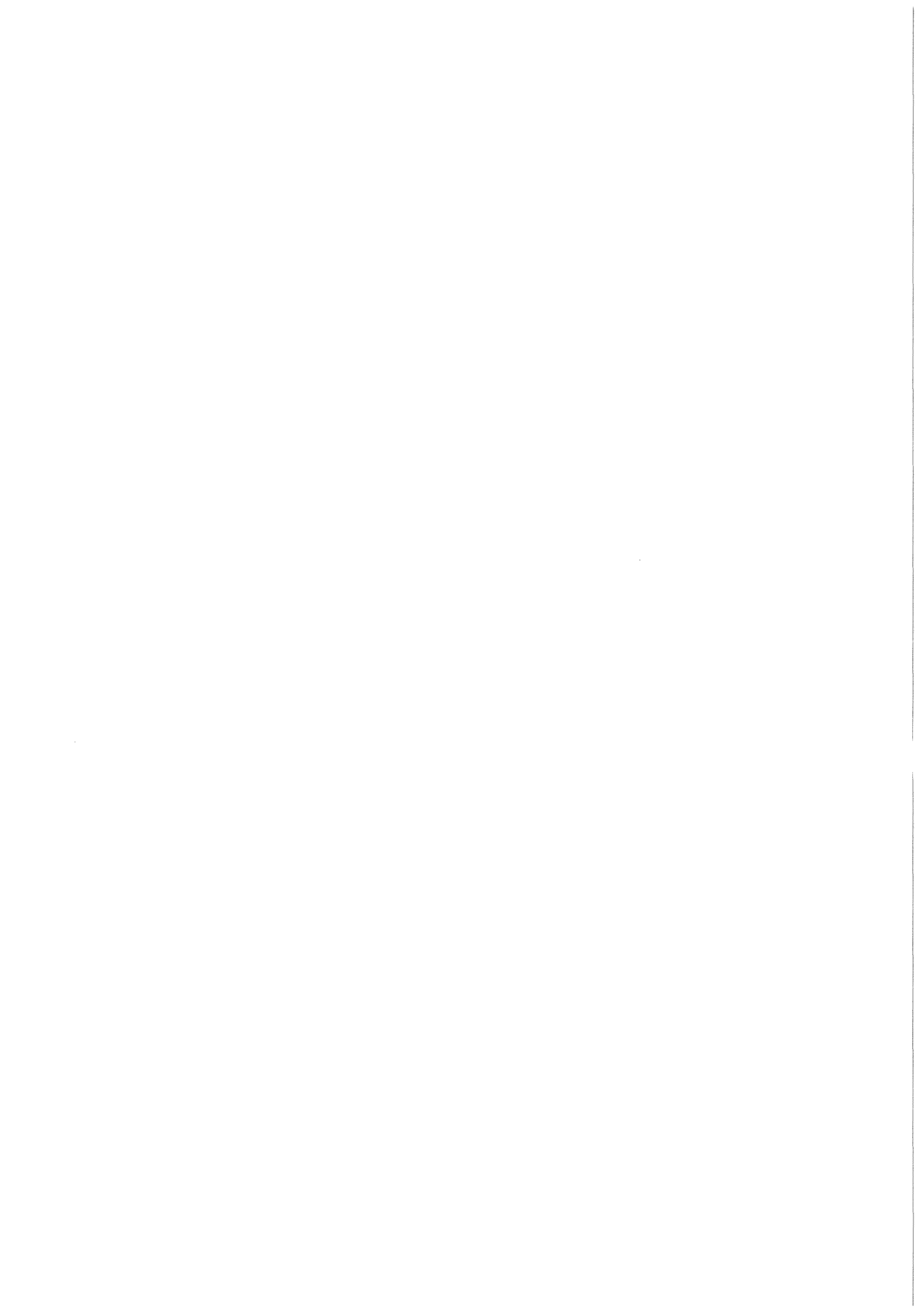


KfK 3412  
November 1982

# Neutron Capture Resonances in $^{56}\text{Fe}$ and $^{58}\text{Fe}$ in the Energy Range from 10 to 100 keV

F. Käppeler, K. Wisshak, L. D. Hong  
Institut für Angewandte Kernphysik

**Kernforschungszentrum Karlsruhe**



KERNFORSCHUNGSZENTRUM KARLSRUHE  
Institut für Angewandte Kernphysik  
KfK 3412

NEUTRON CAPTURE RESONANCES IN  $^{56}\text{Fe}$  AND  
 $^{58}\text{Fe}$  IN THE ENERGY RANGE FROM 10 TO 100 keV

F. Käppeler, K. Wisshak, and L.D. Hong

Kernforschungszentrum Karlsruhe GmbH, Karlsruhe

Als Manuskript vervielfältigt  
Für diesen Bericht behalten wir uns alle Rechte vor

Kernforschungszentrum Karlsruhe GmbH  
ISSN 0303-4003

## ABSTRACT

The neutron capture cross section of  $^{56}\text{Fe}$  and  $^{58}\text{Fe}$  has been measured in the energy range from 10 to 250 keV relative to the gold standard. A pulsed 3 MV Van de Graaff accelerator and the  $^7\text{Li}(p,n)$  reaction served as a neutron source. Capture gamma rays were detected by two  $\text{C}_6\text{D}_6$  detectors, which were operated in coincidence and anticoincidence mode. Two-dimensional data acquisition allowed to apply the pulse height weighting technique off-line. The samples were located at a flight path of 60 cm. The total time resolution was 1.2 ns thus allowing for an energy resolution of 2 ns/m. The experimental set-up was optimized with respect to low background and low neutron sensitivity. The additional flight path of 4 cm from the sample to the detector was sufficient to discriminate capture of sample scattered neutrons by the additional time of flight. In this way reliable results were obtained even for the strong s-wave resonances of both isotopes. The experimental capture yield was analyzed with the FANAC code. The energy resolution allowed to extract resonance parameters in the energy range from 10 to 100 keV. The individual systematic uncertainties of the experimental method are discussed in detail. They were found to range between 5 and 10 % while the statistical uncertainty is 3-5 % for most of the resonances. A comparison to the results of other authors exhibits in case of  $^{56}\text{Fe}$  systematic differences of 7-11 %. For  $^{58}\text{Fe}$  the present results differ up to 50 % from the only other measurement for this isotope.

## ZUSAMMENFASSUNG

Neutroneneinfangresonanzen in  $^{56}\text{Fe}$  und  $^{58}\text{Fe}$  im Energiebereich von 10 bis 100 keV

Der Wirkungsquerschnitt für Neutroneneinfang in  $^{56}\text{Fe}$  und  $^{58}\text{Fe}$  wurde im Energiebereich von 10-250 keV relativ zum Goldstandard gemessen. Neutronen wurden über die  $^7\text{Li}(p,n)$  Reaktion mit dem gepulsten Strahl des 3 MV Van de Graaff

Beschleunigers erzeugt. Die beim Einfang emittierte Gamma-Strahlung wurde mit zwei  $C_6D_6$  Detektoren gemessen, die sowohl in Koinzidenz als auch in Antikoinzidenz geschaltet waren. Mittels zweidimensionaler Datenaufnahme konnte die Methode der Impulshöhenwichtung nach der Messung angewandt werden. Die Proben waren in 60 cm Abstand vom Neutronentarget angeordnet. Die Zeitauflösung betrug 1.2 ns, was einer Energieauflösung von 2 ns/m entspricht. Der experimentelle Aufbau war auf geringen Untergrund und geringe Neutronenempfindlichkeit optimiert. Der zusätzliche Flugweg von 4 cm zwischen Probe und Detektor erlaubte es, Einfangereignisse von gestreuten Neutronen über deren zusätzliche Flugzeit auszusondern. Auf diese Weise konnten auch die starken s-Wellen Resonanzen beider Isotope genau untersucht werden. Die gemessenen Einfangraten wurden mit dem FANAC Programm ausgewertet. Die Energieauflösung erlaubte es, Resonanzparameter im Energiebereich von 10-100 keV zu bestimmen. Die verschiedenen systematischen Unsicherheiten der Meßmethode werden im einzelnen diskutiert. Sie liegen für die meisten Resonanzen zwischen 5 und 10 %, während die statistische Genauigkeit 3-5 % beträgt. Ein Vergleich mit den Daten anderer Autoren ergab für  $^{56}Fe$  systematische Unterschiede von 7-11 %. Im Falle von  $^{58}Fe$  unterscheiden sich die vorliegenden Ergebnisse bis zu 50 % von dem einzigen Datensatz, der bisher veröffentlicht wurde.

## I. INTRODUCTION

The keV neutron capture cross sections of  $^{56}\text{Fe}$  and  $^{58}\text{Fe}$  are of interest for quite different purposes. The isotope  $^{56}\text{Fe}$  is an important structural material and data are therefore requested for fast reactor design studies<sup>1</sup>. On the contrary  $^{58}\text{Fe}$ , which has a natural abundance of only 0.3 %, is an important nucleus in the field of nuclear astrophysics. It is the first isotope in the reaction chain of the slow neutron capture (s)-process following the  $^{56}\text{Fe}$  seed which is predominantly produced in this process. Therefore, it is an important normalization point for s-process calculations around  $A \sim 60$  (Ref. 2).

Several measurements have been performed on  $^{56}\text{Fe}$  at LINAC accelerators using the liquid scintillator tank<sup>3,4</sup>, the  $\text{C}_6\text{F}_6$  detector<sup>5</sup> or the  $\text{C}_6\text{D}_6$  detector<sup>6</sup>. Van de Graaff accelerators in connection with the  $^7\text{Li}(p,n)$  reaction for neutron production offer quite different background conditions and the respective measurements provide data which are widely independent from Linac experiments. There are  $^{56}\text{Fe}$  resonance parameters from one experiment using a liquid scintillator tank<sup>7,8</sup>. In addition, the cross section has been measured by Le Rigoleur et al.<sup>9</sup> using  $\text{C}_6\text{D}_6$  detectors. At present exists a systematic difference of 20 % between the high values of Ref. 5 and the low values of Refs. 4 and 6 which were reanalyzed in Refs. 10 and 11 while the results of Ref. 7 and 8 are somewhere in between these extremes.

For  $^{58}\text{Fe}$  only one set of data has been published until now<sup>12</sup>, measured with a  $\text{C}_6\text{F}_6$  detector at ORELA. This experiment as well as older measurements on  $^{56}\text{Fe}$  (Refs. 3,5) suffered from their high sensitivity to scattered neutrons which made it impossible to deduce reliable data for the broad s-wave scattering resonances. These resonances, however, determine to a large degree the fast reactor averaged capture cross section of  $^{56}\text{Fe}$

as well as the Maxwellian averaged cross section for  $kT=30$  keV of  $^{58}\text{Fe}$ , which is so important for astrophysics.

In the present experiment the Karlsruhe 3 MV Van de Graaff accelerator was used for neutron production via the  $^7\text{Li}(p,n)$  reaction. The samples were located at a flight path of 60 cm, observed by two  $\text{C}_6\text{D}_6$  detectors. The set-up combines a low intrinsic sensitivity to scattered neutrons with the possibility of further discrimination by time-of-flight. The distance from sample to detector is sufficient to separate in the time of flight (TOF) spectra events due to capture of resonance scattered neutrons from the resonance area. Thus the experimental method differ in essential parts from other experiments and the results can be considered to be widely independent as far as systematic uncertainties are concerned.

## II. MEASUREMENTS

During the measurements, the pulsed proton beam of the accelerator was adjusted  $\sim 20$  and or  $\sim 135$  keV above the reaction threshold of the  $^7\text{Li}(p,n)$  reaction. In this way continuous neutron spectra in the energy range from 10 to 80 keV and 5 to 250 keV were obtained at the sample position. The relevant parameters of the neutron source are compiled in Table I.

The experimental set-up was carefully optimized with respect to background conditions in order to allow for measurements of very low cross sections. As a detailed description can be found in Refs. 13 and 14, only a brief discussion is given here. Fig. 1 shows a schematic view of the experiment. The pulsed proton beam hits the metallic lithium target with a diameter of 6 mm. A well defined neutron beam is produced by a 30 cm thick collimating system. This consists of a central cylinder of  $^6\text{Li}$ -carbonate surrounded by a mixture of boron and araldite. This collimator as well as the beam line behind the target is shielded by lithium-loaded paraffin blocks. The target is observed

by a lithium glass neutron monitor at  $90^\circ$  with respect to the beam axis.

Two cylindrical  $C_6D_6$  detectors (each containing 1 liter NE 230; 115 mm diameter, 96 mm thickness) are used for detection of capture gamma rays. They are located at  $90^\circ$  to the beam axis at a distance of 4 cm from the centre of the sample. The scintillator is canned in a 0.5 mm thick aluminium housing and connected with a quartz adapter to a 4 inch photomultiplier (Valvo XP 2041). The detectors are shielded by at least 20 cm of antimony free lead against gamma rays from the lithium target, the collimator and from natural radioactivity. A 0.5 cm thick shielding from  $^6Li$  carbonate reduces background from scattered neutrons which are moderated in the scintillator and thereafter captured in the detector casing, the sample or in surrounding materials.

The four samples used in each run of the measurements were mounted in a low mass sample changer and cycled automatically into the measuring position. The data acquisition time of  $\sim 10$  min/sample is determined by a beam current integrator. The check for equal neutron flux was achieved by integrating the counting rate of the neutron monitor for each sample separately. The following samples were used: (i) the iron sample, (ii) the gold sample and (iii) the carbon sample. To obtain similar background conditions, all samples were enclosed in identical 0.2 mm thick aluminium cannings. To determine the respective background an empty casing was placed in the fourth sample position. Details of the individual samples are compiled in Table II. The electronic consisted of conventional NIM modules and data acquisition was performed using a Nova 2 computer. Pulse height and TOF information of both  $C_6D_6$  detectors was stored in two-dimensional data fields each with  $16 \times 1024$  channels. In this way it was possible to evaluate the data of each detector separately and to apply an appropriate weighting function off line. A special electronic circuit ensured that an event was stored in these data fields only if there was no coincidence between both detectors. Coincident events were accumulated in a separate

one dimensional TOF spectrum. This spectrum was used to estimate the systematic uncertainty due to pile-up events and to get a rough information on multiplicity and hardness of the capture gamma-ray spectra in individual resonances. The total time resolution of accelerator and detectors was 1.2 ns and consequently at a flight path of 60 cm an energy resolution of 2.0 ns/m was obtained. This was sufficient to resolve most of the resonances in both iron isotopes in the energy range from 10 to 100 keV. On the other hand the flight path was sufficiently short that sample scattered neutrons appeared in the TOF spectra with a sufficient delay compared to the scattering resonance to be discriminated. For example, neutrons scattered in the 27.7 keV resonance in  $^{56}\text{Fe}$  have a primary TOF of 261 ns and need at least further 17 ns to reach the detector. A TOF of 278 ns corresponds to a primary neutron energy of 24.4 keV which is clearly outside the resonance area.

During the measurements on  $^{58}\text{Fe}$  two different proton energies were chosen resulting in continuous neutron spectra ranging from 10-80 keV and 5 to 250 keV, respectively. As the time independent background has a strong component which is proportional to the integrated neutron flux, the narrower energy range offers an improved signal to background ratio. Two independent runs have been performed with each of the two neutron spectra. The measurements on  $^{56}\text{Fe}$  were performed with neutrons in the wider energy range only.

Several additional measurements were carried out to reduce systematic uncertainties. In order to investigate the background due to strong scattering resonances, separate runs have been performed with thick samples of sodium ( $E_r=53$  keV) and aluminium, ( $E_r=35$  keV). With the geometric arrangement of the present experiment, gamma-ray self absorption in the samples turned out to be a significant effect, especially in the relatively thick (1 mm) gold reference sample. Therefore, accurate measurements have been performed at a fixed neutron energy using

gold samples with thicknesses between 0.15 mm and 1.5 mm (Ref. 15).

### III. DATA ANALYSIS

#### a) Determination of the Capture Yield

The capture yield was evaluated from the measured spectra by the following steps:

##### 1) Transformation to a common time scale:

The position of the prompt gamma-ray peak in the TOF spectra, which was used as a normalization point for the energy determination varied slightly with the measuring time and with the pulse height channel. Therefore all TOF spectra of all the individual measurements (corresponding to the 10 min measuring time) were shifted to a common gamma peak position. In this way for each sample a total TOF spectrum with improved resolution was obtained. Then, the spectra of both detectors were added.

##### 2) Weighting of the spectra:

One dimensional TOF spectra were obtained by multiplying each pulse height channel with the appropriate value of the weighting function. The weighting function for the geometry of the present experiment was calculated by Hensley<sup>16</sup> using a modified version of a code from Le Rigoleur<sup>17</sup>. The calculation was repeated with the code of Macklin<sup>18</sup>. Very good agreement in the shape of the weighting function was found from the two calculations. In addition, the agreement to the weighting functions used in Geel and Harwell as taken from Ref. 19 is better than 3 %.

In Figs. 2 and 3 the resulting TOF spectra for  $^{56}\text{Fe}$  ( $E_n^{\text{max}} = 250 \text{ keV}$ ) and  $^{58}\text{Fe}$  ( $E_n^{\text{max}} = 80 \text{ keV}$ ) are shown together with the respective spectra of the other samples.

### 3) Background subtraction

In a first step, the background spectrum measured with the empty canning was subtracted from the TOF spectra of all other samples. In the second step events due to capture of scattered neutrons were subtracted using the TOF spectrum of the carbon sample which is only due to scattering. This spectrum was normalized to the respective gold and iron spectra in a region on the right of the prompt gamma-ray peak (channels 970-1010 see Fig. 2 and 3). In this region the background due to scattered neutrons is time-independent and only proportional to the scattering cross section averaged over the neutron flux of the continuous spectrum. Therefore, the normalization constant  $\alpha$  can be calculated according to the relation

$$\alpha = \frac{N_I}{N_C} \cdot \frac{\int \sigma_{nn,I}(E) \phi(E) dE}{\int \sigma_{nn,C}(E) \phi(E) dE} \quad (1)$$

- N = Number of atoms in the sample
- $\sigma_{nn}$  = scattering cross section
- $\phi$  = shape of the neutron flux
- I = index for  $^{197}\text{Au}$ ,  $^{56}\text{Fe}$ ,  $^{58}\text{Fe}$
- C = index for carbon

The transmission of the gold and the carbon sample was 94 % and 76 %. To account for this finite transmission, an effective number of atoms N was assumed which was lower than the actual number of atoms by 3 % for the gold and by 12 % for the carbon sample. For the iron samples the calculation of  $\alpha$  is relatively uncertain as only averaged scattering cross sections were considered by the program but not the detailed resonance structure. In this case, however,  $\alpha$  can be determined experimentally from the condition that the cross section between resonances is practically zero at very low energies (5-6 keV). In this region of the TOF spectra the low neutron yield caused the signal-to-background ratio to drop almost to zero and therefore the cross section shape is very sensitive to  $\alpha$ .

That this procedure of background subtraction is applicable also for the iron isotopes with their strong scattering resonances was verified by measurements on thick sodium and aluminium samples which proved that the background caused by strong scattering resonances has the same time dependence as the background measured with the carbon sample.

Before subtraction, the carbon spectrum was smoothed by fitting a high order polynomial to the experimental data. This part of the evaluation is illustrated in Figs. 4 and 5.

#### 4) Normalization to the gold standard

In the determination of the capture yield from a relative measurement using a gold standard, problems arise due to structures in the gold cross section. Especially in  $^{58}\text{Fe}$ , structures at low energies coincide with strong resonances (e.g., at 10 keV and 19 keV).

In order to get reliable results for the parameters of individual resonances the evaluation has been performed in three different ways.

- (i) The experimental TOF spectrum of the gold sample was smoothed strongly and the smooth cross section from ENDF/B-IV was taken as a reference.
- (ii) The TOF spectrum of the gold sample was smoothed slightly and the cross section was taken from ENDF/B-V, averaged over 1 keV intervals.
- (iii) The TOF spectrum of the gold sample was used without smoothing and the cross section from ENDF/B-V was taken with full resolution.

The second procedure was necessary as an intermediate step because the very narrow structures in the gold cross section at low energies did not coincide exactly with the respective structures in the TOF spectra, if procedure (iii) was applied due to uncertainties in the energy scale of the present experiment.

The respective gold spectra and standard cross sections are shown in Fig 6. The solid lines in the experimental TOF spectrum represent the counting rates used in the actual analysis. The capture yields obtained with the three different methods were used in the final resonance analysis and the observed differences for the individual resonances led to a reliable estimate of the systematic uncertainty corresponding to this effect.

5) Correction for multiple scattering and resonance self-shielding in the gold sample

The correction for multiple scattering and self-shielding in the gold sample was calculated using the SESH code of Fröhner<sup>20</sup>. The results obtained for a sample with 40 mm diameter and 1 mm thickness are given in Table III. The quoted accuracy is the accuracy of the Monte Carlo simulation and does not include systematic uncertainties due to uncertainties in the input parameters. A linear interpolation was used to calculate the respective correction for each TOF channel.

6) Correction for gamma-ray self-absorption

The gamma ray self-absorption in gold has been measured by observing the capture yield as a function of sample thickness<sup>15</sup>. A correction factor  $SA_{\text{gold}} = 0.89$  was obtained for the gold sample of the present experiment. The respective correction for the iron samples was calculated with the following assumptions:

- (i) Gamma energies below 1 MeV are neglected as they are strongly suppressed by the weighting function.
- (ii) The ratio of the absorption coefficients  $\mu(\text{Au})/\mu(\text{Fe})$  is constant in the energy range from 1 to 7 MeV.
- (iii) The average total energy absorption  $\mu(\text{TOTA})$  of gold is  $\mu(\text{TOTA}) = 8.9$  b/atom while the respective value for iron is 2.0 b/atom according to Ref. 21.

With the geometry of the present experiment the gamma-ray self-absorption is strongly dependent on the emission angle. In order to account for this specific geometry, we normalized the self absorption correction for the iron samples by means of two idealized cases for which SA can be derived by analytical expressions<sup>22</sup> :

- (i) An infinite slab sample of thickness X1 parallel to the detector surface and
- (ii) an infinite cylindrical sample of radius X2 with the axis parallel to the detector surface.

For the gold sample the experimental correction factor SA=0.89 corresponds to X1 = 4.3 mm and X2=2.8 mm, which means that the idealized samples appear to be 4.3 and 5.6 times thicker than the actual gold sample. These factors contain all the information on the difference between the experimental and the idealized geometry. The self absorption correction factors SA for the iron samples are now calculated backward by increasing the actual sample thicknesses by the above factors and applying then the analytical expressions for the idealized geometries. In that way we find consistent self absorption corrections, both for <sup>56</sup>Fe (SA<sub>1</sub> = 0.964, SA<sub>2</sub> = 0.961,  $\overline{SA}$  = 0.962) and for <sup>58</sup>Fe ( $\overline{SA}$ =0.950).

Finally, the capture yield is calculated according to the relation:

$$Y_I = \frac{C_I}{C_{Au}} \cdot \frac{N_{Au}}{N_I} \cdot \frac{B_{Au}}{B_I} \cdot \frac{SA_{Au}}{SA_I} \quad MS \times SS_{Au} \sigma_{Au} \quad (2)$$

C = background corrected counting rate of the pulse height weighted TOF spectrum

N = Number of atoms in the sample

B = neutron separation energy

SA= correctionfor gamma-ray self-absorption

MSxSS = correction for neutron multiple scattering and self-shielding

$\sigma$  = standard cross section  
I = index for  $^{56}\text{Fe}$  and  $^{58}\text{Fe}$   
Au = index for gold.

### 7) Evaluation of Coincidence Spectra

The TOF spectra of coincident events were evaluated in the same way as described above. As only one dimensional spectra have been recorded, no pulse height weighting could be applied. Therefore, the obtained yields can only be taken as relative numbers for investigating differences between individual resonances of one isotope.

### b) Determination of Resonance Parameters

Resonance parameters were extracted from the measured capture yield by means of the FANAC code of Fröhner<sup>23</sup>. As the  $^{58}\text{Fe}$  sample was only enriched to 77 % and as natural  $^{56}\text{Fe}$  was used, all known resonances of  $^{54,56,57,58}\text{Fe}$  were included in each fit. The resonance parameters of the respective impurity isotopes were taken as fixed parameters from Ref. 24. In case of  $^{58}\text{Fe}$ , also oxygen was included in the fit. The strength functions and nuclear radii that were also required as input for the code are compiled in Table IV. These data were taken from Ref. 24 and 25. As in the evaluation of the capture yield the binding energy of the main isotope was used (eq. 2), the capture area of the impurity isotopes was normalized in the fit by the ratio of the binding energies of the respective impurity isotope and the main isotope.

It was mentioned earlier that scattering in the broad s-wave resonances caused a smooth time-dependent background with the same shape as the graphite spectrum. This holds with only one exception: Part of the neutrons scattered in the broad  $^{58}\text{Fe}$  resonance at 43.4 keV ( $\Gamma_n = 4.9$  keV) overlap in energy with the 35.3 keV resonance in  $^{27}\text{Al}$ . In this case capture in the aluminium cans of the  $\text{C}_6\text{D}_6$  detectors leads to a time-dependent background well separated from the resonance area but not accounted

for by the background subtraction as described above. This additional background was fitted assuming an artificial isotope with broad resonances in the energy region from 18 to 35 keV.

In case of  $^{58}\text{Fe}$  the results of four independent runs were fitted separately in order to check for inconsistencies. As none were found, the final fits were performed after summation over all runs. Nevertheless, the results obtained from the three different normalizations to the gold standard were analyzed independently. In Figs. 7 and 8 the final FANAC fits for  $^{56}\text{Fe}$  and  $^{58}\text{Fe}$  in the energy range from 10 to 100 keV are shown. The dashed line is the contribution of impurity isotopes and the aluminium background discussed above. Especially in the case of  $^{58}\text{Fe}$  it can be seen from Fig. 8 that the isotopic impurities are very well accounted for by the resonance parameters of Ref. 24.

The coincidence yield was analyzed accordingly. In this case the efficiency is proportional to the square of the binding energies. As this was not accounted for in eq. 2, the area of all resonances was normalized by a factor  $B_{\text{Au}}/B_{\text{I}}$  ( $\text{I} = ^{56}\text{Fe}, ^{58}\text{Fe}$ , respectively). For the impurity isotopes an additional factor  $(B_{\text{I}}/B_{\text{J}})^2$  had to be applied, J being the index for the impurity isotope. The final fits of the coincidence spectra are shown in Figs. 9 and 10.

#### IV. RESULTS

The results for the neutron resonances of  $^{56,58}\text{Fe}$  in the energy range from 10 to 100 keV are compiled in Tables V and VI. A statistical uncertainty of 3-6 % was obtained for most of the resonances. The systematic uncertainties, which are discussed in detail in section V are 5-8 % on the average. In the last column of Tables V and VI the ratio R of the resonance area as determined from the coincidence and anticoincidence spectra of both detectors are given.

1. Results for  $^{56}\text{Fe}$

If we compare the present results for  $^{56}\text{Fe}$  with previous measurements, we find on the average good agreement with the data of Ernst and Fröhner<sup>7,8</sup> for energies below  $\sim 90$  keV while our data are  $\sim 20$  % higher above. However, a similar effect is observed as discussed already by Rohr<sup>26</sup> for the respective comparison with the CBNM (Ref. 6,10) and ORNL-AAEC data (Ref. 5). The difference to the data of Ernst and Fröhner is dependent from hardness and/or multiplicity of the capture gamma-ray spectrum of the respective resonance. We observe that for all resonances with  $R < 0.4$  (hard gamma spectrum and/or low multiplicity) our results are larger by 6-20 % and for resonances with  $R > 0.4$  (soft gamma spectrum and/or high multiplicity) our results are smaller by 4-18 %. According to a statistical model calculation<sup>27</sup> the average gamma-ray multiplicity for p and d wave resonances is  $\sim 3$ . Therefore it seems more likely that the systematic uncertainty observed arises in a tank measurement as the efficiency of a tank is much different for an event with e.g. multiplicity 2 or 3. In case of the pulse height weighting technique a much smaller dependence of the efficiency from gamma-ray multiplicity is expected. Good agreement is also obtained with the KEDAK-3 evaluation<sup>24</sup>. The remaining differences are within the respective uncertainties and for the average over 22 resonances the systematic difference is only  $\sim 2$  %. Compared to the preliminary values of Brusegan et al.<sup>6,10</sup> our data are systematically higher by  $\sim 11$  % (e.g. for the average over the 15 resonances between 20 and 84 keV). But if this systematic difference is taken into account both data sets agree remarkably good in the individual resonance parameters.\* A similar trend is found in comparing our results to the data of Gayther et al.<sup>11</sup>. Below 40 keV where the data sets overlap our values are higher by  $\sim 20$  %. With respect to the results of Allen et al.<sup>5</sup> we find a systematic discrepancy in the opposite direction: our average over 21 resonances is lower by  $\sim 7$  % (excluded the 27.7 keV resonance, which is certainly disturbed by scattered neutrons in Ref. 5).

---

\* See note added in manuscript on page 21

In these comparisons, the 27.7 keV resonance deserves special attention. It was pointed out earlier that our experimental set-up provides the resonance area completely undisturbed by capture of scattered neutrons. The present results  $\Gamma_{\gamma}=1.04$  eV is in excellent agreement with measurements using Moxon-Rae detectors in connection with TOF discrimination of scattered neutrons at very short flight paths<sup>28,29</sup>. Good agreement is further found with the preliminary value of the Geel group\* given in Ref. 10 and with the KEDAK 3 evaluation<sup>24</sup>. The data of Gayther et al.<sup>11</sup> and Allen et al.<sup>27,30</sup> are systematically lower, while in the older measurements<sup>3,5</sup> much larger values were obtained, very likely due to incomplete corrections of the neutron sensitivity.

In our final fits the neutron width of the 27.7 keV s-wave resonances was treated as a free parameter and a value of  $\Gamma_n = 1.45$  keV was obtained. This is consistent with the neutron widths from literature<sup>8,31,32,33</sup> where values between 1.40 keV and 1.52 keV are quoted. This demonstrates that the present method is able to reproduce the neutron width with an accuracy of ~5-10 % in spite of the rather poor energy resolution. The neutron widths of all other s-wave resonances in <sup>56</sup>Fe were used as fixed parameters and were adopted from KEDAK 3.

## 2. Results for <sup>58</sup>Fe

For <sup>58</sup>Fe only one set of resonance parameters has been published until now by Allen and Macklin<sup>12</sup>. Recently these authors found an error in their data analysis and have revised their first results by a correction factor 0.9655 (Ref. 34). The further discussion therefore refers always to the corrected values of Allen and Macklin<sup>12</sup>. A comparison to these data is difficult because of the following reasons:

- (i) in their measurement the sensitivity to scattered neutrons is so large that for s-wave resonances only very rough estimates could be given (the quoted statistical uncertainties for the resonances at 43.3 keV and 93.0 keV are 100 %).
- (ii) The correction for isotopic impurities was not performed properly<sup>35</sup>. This can be seen from the fact that in the energy range from 10 to 100 keV nine resonances are given with energies corresponding to resonances in <sup>56</sup>Fe. Consequently, much lower

\* See note added in manuscript on page 21

values are found in the present work for all resonances which are close to resonances in isotopic impurities (e.g. at 34.6, 45.8, 53.3 and 97.9 keV).

(iii) The value for the resonance at 29.27 keV is obviously misprinted and by a factor of 10 too low.

For these reasons a comparison to the data of Ref. 12 can be made only for nine resonances that are not affected by the above points. The results for individual resonances differ by  $\pm 15\%$ , but there is practically no systematic difference for the average of all resonances.

As can be seen from Fig. 8, the isotopic impurities are well reproduced in our fits with the resonance parameters from KEDAK 3. There is probably an additional weak resonance at 21.3 keV with  $g\Gamma_n\Gamma_\gamma/\Gamma \approx 0.03$ . The resonance at 53.5 keV was evaluated assuming  $g\Gamma_n\Gamma_\gamma/\Gamma = 0.439$  for the resonance  $^{24}$  in  $^{56}\text{Fe}$  with the same energy. This value is relatively large compared to the present results for  $^{56}\text{Fe}$  as well as compared to the measurements in Geel<sup>10</sup> and Oak Ridge<sup>5</sup>. Therefore the area of this resonance in  $^{58}\text{Fe}$  might be somewhat larger than the value given in Table VI. Above  $\sim 80$  keV the evaluation of our data was difficult due to the limited energy resolution. In order to obtain convergence in the fits,  $\Gamma_\gamma$  of the broad resonance at 93.0 keV had to be taken as a fixed parameter. Therefore, an uncertainty of  $\sim 20\%$  must be assigned to that value ( $\Gamma_\gamma = 1$  eV).

It was stated before that the neutron widths  $\Gamma_n$  of s-wave resonances can be determined from our data with an uncertainty of  $\sim 10\%$ . Hence, the present results for the resonance at 10.4, 43.3 and 68.5 keV may be used to solve the severe discrepancy between the data of Beer et al.<sup>36</sup> and Garg et al.<sup>37</sup>, strongly favouring the latter data.

### 3. The ratio of coincident and single events

$$\text{The ratios } R = \frac{\text{resonance area measured with both detectors in coincidence}}{\text{resonance area measured with both detectors in anticoincidence}}$$

are given in the last column of Tables V and VI. They are determined

by the average multiplicity and by the hardness of the capture gamma-ray spectra of the individual resonances. As the coincidence spectra have not been weighted, different average values for  $R$  were obtained for both iron isotopes and the values can be compared quantitatively only within one isotope. Small values of  $R$  indicate a lower multiplicity and/or a harder gamma-ray spectrum for the respective resonance.

The values for  $R$  can qualitatively be compared with the ratio  $\bar{w}$  of weighted to unweighted resonance intensities given for  $^{56}\text{Fe}$  by Brusegan et al.<sup>6</sup>. The same variation is found for the individual resonances if one keeps in mind that small  $R$  values correspond to large  $\bar{w}$  values. However, due to the observation of coincidences between both detectors the sensitivity of the  $R$  values to different multiplicity and/or hardness of the spectrum is much better: the  $R$  values vary by a factor of 7 for different resonances, while the respective  $\bar{w}$  values vary only by a factor of two. In  $^{56}\text{Fe}$  the  $R$  values seem to cluster around certain regions as e.g.  $R = 0.4 \pm 0.02$  and  $R = 0.27 \pm 0.02$  whereas from a statistical viewpoint one would expect a more smooth behaviour. There is no significant evidence that this structure correlates to definite spin states, if we adopt the resonance spins from Ref. 31. However, the fact that four of five resonances with  $R \approx 0.27$  in  $^{56}\text{Fe}$  have spin  $3/2^-$  whereas no such spin, is observed in the cluster of 8 resonances with  $R \approx 0.4$  may be a weak indication in this direction. In  $^{58}\text{Fe}$  a cluster of 5 resonances is observed for  $R = 0.62 \pm 0.03$ .

## V. DISCUSSION OF UNCERTAINTIES

The systematic uncertainties of the present experiment have been evaluated in detail and the results are compiled in Tables VII and VIII. These tables contain the uncertainties that depend on resonance strength and energy, while the uncertainties common to all resonances are given in Table IX.

### 1. Background subtraction

The accuracy of background subtraction in the present experiment is dominated by the uncertainty of the factor  $\alpha$

(see eq. (1)). Two different methods have been applied to fix this quantity for the spectra of the iron isotopes.

(i)  $\alpha$  was calculated using the shape of the neutron flux as obtained from the ratio of the gold spectrum and the gold capture cross section. The scattering cross section was taken from the literature.

(ii) In the process of data analysis  $\alpha$  was chosen such that the final cross section was practically zero between the resonances at very low energies. This is a very sensitive method and small deviations from the correct value immediately show up in an unphysically increase or decrease of the cross section between 5 and 6 keV.

The first method allowed for an accuracy of  $\sim 8\%$  while with the second method  $\alpha$  could be fixed to within  $\pm 3\%$ . To evaluate the systematic uncertainties given in Table VII and VIII, the optimum  $\alpha$  values of each run were varied by  $\pm 5\%$ . For the gold spectra only the first method could be applied and an accuracy of  $\pm 10\%$  was assumed for the  $\alpha$  values obtained.

In case of  $^{58}\text{Fe}$  an additional time-dependent background was subtracted that was caused by the overlap of the 43.3 keV scattering resonance and the 35.3 keV resonance of the aluminium detector canning. This background which affects the resonances in the energy range from 19 to 38 keV (see Fig. 8) was assumed to have an uncertainty of 20 %.

## 2. Weighting function

The shape of the weighting function of the  $\text{C}_6\text{D}_6$  detectors is known with very good accuracy as different computer codes yield results which agree to better than  $\sim 3\%$  (Refs. 16,19). What is generally not considered in this context is the fact that the energy scale is afflicted with relatively large uncertainties in actual experiments. The energy calibration is performed using the Compton edge of standard sources and there is in general the problem of correctly defining the Compton edges. In addition, monoenergetic gamma-ray sources are not easily available at high energies so that the calibration is usually extrapolated

above  $\sim 2$  MeV. In the present experiment  $^{85}\text{Sr}$ ,  $^{65}\text{Zn}$  and  $^{60}\text{Co}$  sources were used and it was assumed that the energy scale was fixed with an accuracy of  $\pm 1$  MeV at 10 MeV.

To obtain the respective systematic uncertainty the energy scale of the weighting function was modified in the above limits and the change in area of each resonance were investigated. The correlated uncertainties are given in column 4 of Tables VII and VIII. Due to the different hardness of the capture gamma ray spectra of individual resonances and the different binding energies of  $^{56}\text{Fe}$  and  $^{58}\text{Fe}$  the uncertainties are differing in a wide range between 0.1 and 2 %.

### 3. Structure in the gold cross section

The systematic uncertainty due to structure in the gold cross section (column 5 of Tables VII and VIII) is the averaged difference of the resonance areas obtained with the three evaluation methods described in section III. An additional uncertainty of 2.5 % was included for the uncertainty of the gold cross section (see Table IX).

### 4. Isotopic impurities

As can be seen from Figs. 7 and 8 some resonances are severely affected by isotopic impurities especially in  $^{58}\text{Fe}$ . To calculate the respective systematic uncertainties (column 6 of Tables VII and VIII) a 10 % uncertainty was assumed for the resonances of the isotopic impurities taken from KEDAK-3.

### 5. Gamma-ray self-absorption and multiple scattering

The correction factor for gamma-ray self-absorption in the gold sample has been measured with an accuracy of 1 % (Ref. 15). As the correction itself is  $\sim 10$  % of the net count rate

the uncertainty of the correction is also 10 %. The gamma-ray self absorption correction for the iron samples was only ~5 %. If we assume an uncertainty of 20 % for the method how that correction was derived (see Sec. III), we end up with a total systematic uncertainty of 1.4 % for the cross section ratio.

As can be seen from Table III typical uncertainties of the multiple scattering and self-shielding correction calculated with the SESH code<sup>20</sup> are < 1 %. A detailed study with different sets of input parameters<sup>38</sup> showed that 1 % can also be adopted as the total systematic uncertainty of this correction.

#### 6. Pile-up events and gamma detector threshold

Pile-up events where two or more capture gamma rays are registered simultaneously in one detector are weighted with a wrong value. This holds for all detectors with weighting functions that do not linearly increase with gamma-ray energy. The present set-up allows to estimate this effect because the number of pile-up events is the same as of the observed coincident events. A detailed investigation was performed in Ref. 14 for a measurement of isotopic neon cross sections relative to gold yielding an uncertainty of 2 %. That same uncertainty is assumed for the present experiment.

The threshold of the gamma-ray detector of ~50 keV introduces a systematic uncertainty in the measured cross section ratio. This is due to the fact that the capture gamma-ray spectrum of gold exhibits - in contrast to the iron isotopes - an intense soft component<sup>29,39</sup>. The corresponding uncertainty was also evaluated in Ref. 14 and is less than 1 %.

#### 7. Neutron flux

It was verified experimentally that the integrated neutron flux was the same for each sample with an accuracy of better than 1 %.

8. Fanac-fit

The effect of the uncertainties of the fixed parameters in the calculation with the FANAC code was studied in detail in Ref. 28. It was found that these uncertainties contribute less than 2 % to the investigated resonance parameters.

Uncertainties due to second order effects were neglected, e.g., for nonisotropic angular distributions of capture gamma rays or for resonance capture of scattered neutrons in the canning.

VI. MAXWELLIAN AVERAGE CROSS SECTIONS

For the investigation of element synthesis by the s-process<sup>40</sup> neutron capture cross sections are required as input data. As the helium burning shell of Red Giant Stars is commonly considered as the site for the s-process, this means that one must assume a Maxwellian neutron energy distribution for a thermal energy of  $kT \sim 30$  keV corresponding to a mean temperature between 300 and 400 million K. According to the conventions in the literature<sup>41</sup> the effective average cross section in such a scenario is given by

$$\frac{\langle \sigma v \rangle}{v_T} = \frac{1}{v_T} \int_0^{\infty} \sigma(v) v \phi(v) dv, \quad (3)$$

where  $\phi(v)$  is the Maxwellian velocity distribution. The thermal velocity  $v_T = (2 kT/m)^{1/2}$  is expressed by the temperature and the reduced mass  $m$ . Due to the shape of the Maxwellian velocity distribution, the limits of integration can be restricted to the energy range between 1 and  $\sim 200$  keV. The most significant part of this region is covered by the present measurement.

For resonant cross sections eq. (3) can be replaced by<sup>42</sup>

$$\frac{\langle \sigma v \rangle}{v_T} = \sigma_{th} \left( \frac{25.3 \cdot 10^{-6}}{kT} \right)^{1/2} + \frac{2}{\sqrt{\pi}} \sum_r A_r \frac{E_r}{(kT)^2} \exp\left(-\frac{E_r}{kT}\right) \quad (4)$$

where the first term accounts for the effect of distant resonances,

$\sigma_{th}$  being the capture cross section at  $kT = 0.0253$  eV.  $A_r$  is the resonance area and  $E_r$  the resonance energy. We have calculated the Maxwellian average cross section for  $^{56}\text{Fe}$  and  $^{58}\text{Fe}$  from the resonance parameters given in Tables V and VI which have been complemented with the parameters of lower lying resonances. These resonances contribute 3 % and 5 % to the 30 keV average cross section of  $^{56}\text{Fe}$  and  $^{58}\text{Fe}$ , respectively. The contributions from resonances above our resolved energy range are much smaller. This was verified at the example of  $^{56}\text{Fe}$  where we calculated the 30 keV average from our resonance parameters ( $E_r^{\max} = 112.6$  keV) and from a second set including the known higher resonances up to  $E_r^{\max} = 192.7$ . Both results agreed to within  $\pm 1$  %.

The Maxwellian average cross sections are listed in Table X for thermal energies between 20 and 40 keV. At 30 keV we have also calculated the overall uncertainty which is 7.6 % for  $^{56}\text{Fe}$  and 10.0 % for  $^{58}\text{Fe}$ . The main contribution to the total uncertainty comes from the systematic uncertainties of the individual resonance parameters (6.0 % for  $^{56}\text{Fe}$  and 8.9 % for  $^{58}\text{Fe}$ ) and from the additional 4.4 % systematic uncertainty which is common to all resonances (Table IX). The statistical uncertainties are comparably small (1.4 and 1.5 % for  $^{56}\text{Fe}$  and  $^{58}\text{Fe}$ ).

It should be noted that the broad s-wave resonances constitute a considerable fraction of the Maxwellian average cross section: 21 % in  $^{56}\text{Fe}$  and 41 % in  $^{58}\text{Fe}$ . It seems that this fact was neglected in the error analysis of Allen and Macklin<sup>12</sup> who had to claim uncertainties of  $\sim 100$  % for broad s-wave resonances. As an example, we find that the three resonances in  $^{58}\text{Fe}$  at 43.3, 66.7 and 93 keV account for 17 % of the Maxwellian average at 30 keV. For these resonances alone the uncertainties of Ref. 12 imply an uncertainty of 15 % for  $\langle\sigma v\rangle/v_T$ . Together with additional systematic uncertainties and the contribution from the other resonances one might expect a larger overall uncertainty than their quoted value of 10 %.

The new result for the 30 keV average of  $^{58}\text{Fe}$  is significantly lower than the value of  $18 \pm 3$  mb deduced from previous work<sup>2</sup>, but agrees very well with the revised cross section of  $15.4 \pm 1.5$  mb by Allen and Macklin<sup>12,34</sup>. The consequences for the s-process  $\sigma_{\text{N}}$ -systematics are that - very likely - the seed abundance for the fluence component  $\rho_1$  must be reduced accordingly. Under the assumptions of Ref. 2 now 2.2 % of the solar  $^{56}\text{Fe}$  abundance should be sufficient as a seed for the component  $\rho_1$  instead of the 2.7 % claimed previously. A more exact and probably even lower value will be available after a study is carried out which considers not only  $^{56}\text{Fe}$  but also  $^{58}\text{Ni}$  and eventually  $^{57}\text{Fe}$  and  $^{60}\text{Ni}$  as seed nuclei for the s-process.

#### ACKNOWLEDGEMENT

We appreciate very much the help of G. Rupp and D. Roller throughout these measurements. We are also indebted to J. Almeida and G. Walter for many discussions during data analysis. The authors would like to acknowledge the support of the U.S. Energy Research and Development Administration in making available the  $^{58}\text{Fe}$  sample material.

#### Note added in manuscript

At the international conference on Nuclear Data for Science and Technology, Antwerp, September 6 - 10, 1982, Corvi et al. reported new data on  $^{56}\text{Fe}$  measured with an improved setup, which should replace the preliminary results from Ref. 6 and 10. These new data are systematically higher than the old data and consequently a much better agreement is found to the present data (for the average over the 15 p-wave resonances between 20 and 84 keV the difference is less than 2 %). For the s-wave resonances much lower values are reported in the new measurement of the CBNM group than were given in Refs 6 and 10 due to the preliminary correction for neutron sensitivity. These values are significantly lower by 20 - 30 % than the present results.

REFERENCES

1. D.W. MUIR, Ed. WRENDA 79/80, World Request List for Nuclear Data INDC(SEC)-73/URSF International Atomic Energy Agency, Vienna, 1979.
2. F. KÄPPELER, H. BEER, K. WISSHAK, D.D. CLAYTON, R.L. MACKLIN and R.A. WARD, Ap. J. 257, 821 (1982).
3. R.W. HOCKENBURY, Z.M. BARTOLOME, J.R. TATARCZUK, W.R. MOYER, and R.C. BLOCK, Phys. Rev. 178, 1746 (1969).
4. D.B. GAYTHER, B.W. THOMAS, B. THOM and M.C. MOXON, Proc. Specialists Meeting on Neutron Data of Structural Materials for Fast Reactors, Geel, Belgium, December 5-8, 1977, p. 547, Pergamon Press, Oxford (1979).
5. B.J. ALLEN, A.R. De L. MUSGROVE, J.W. BOLDEMAN, M.J. KENNY, and R.L. MACKLIN, Nucl. Phys. A 269, 408 (1976).
6. A. BRUSEGAN, F. CORVI, G. ROHR, R. SHELLEY and T. van der VEEN, Proc. Int. Conf. on Nuclear Cross Sections for Technology, Knoxville, Tenn., October 22-26, 1979, NBS Spec. Publ. 594, National Bureau of Standards, Washington, D.C., 1980.
7. A. ERNST, F.H. FRÖHNER, and D. KOMPE, Proc. 2nd Int. Conf. Nuclear Data for Reactors, Helsinki, June 15-19, 1970, CONF-700605, Vol. I p. 619, International Atomic Energy Agency (1970).
8. F.H. FRÖHNER, Proc. Specialists Meeting Neutron Data of Structural Materials for Fast Reactors, Geel, Belgium, December 5-8, 1977, p. 138, Pergamon Press, Oxford (1979).
9. C. Le RIGOLEUR, A. ARNAUD, and J. TASTE, "Mesures en Valeur Absolue des Sections Efficaces de Capture Radiative des Neutrons par le  $^{23}\text{Na}$ , Cr,  $^{55}\text{Mn}$ , Fe, Ni,  $^{103}\text{Rh}$ , Ta,  $^{197}\text{Au}$ ,  $^{238}\text{U}$  dans le Domaine de 10 a 600 keV", CEA-R-4788 Commissariat a l'Energie Atomique, Saclay, France (1976).
10. M.C. MOXON, U.K. Nuclear Data Progress Report for the Period, January to December 1980", UKNDC(81)P100, NEANDC(E) 222 Vol. 8 INDC(UK) - 35/LN United Kingdom Atomic Energy Authority, Harwell 1981.

11. D.B. GAYTHER, M.C. MOXON, R.B. THOM and J.E. JOLLY  
U.K. Nuclear Data Progress Report for the Period  
January to December 1979, UKNDC(80)P96, NEANDC(E)212,  
INDC(UK)-32/LN United Kingdom Atomic Energy Authority,  
Harwell 1980.
12. B.J. ALLEN and R.L. MACKLIN, J. Phys. G: Nucl. Phys. 6,  
318 (1980).
13. B. LEUGERS, "Die Neutroneneinfangquerschnitte der Krypton-  
isotope und ihre Bedeutung für die Astrophysik", KfK 2895,  
Kernforschungszentrum Karlsruhe, 1979.
14. J. ALMEIDA, "The Capture Cross Sections of the Neon  
Isotopes and the s-Process Neutron Balance", KfK 3347,  
Kernforschungszentrum Karlsruhe 1982.
15. G. WALTER, K. WISSHAK and F. KÄPPELER, to be published.
16. F. HENSLEY, "Eine Methode zur Bestimmung der Neutroneneinfang-  
querschnitte von Kryptonisotopen, KfK 2918, Kernforschungs-  
zentrum Karlsruhe, 1980.
17. C. Le RIGOLEUR, unpublished results.
18. R.L. MACKLIN and J.H. GIBBONS, Phys. Rev. 159, 1007 (1967).
19. R.B. THOM, "U.K. Nuclear Data Progress Report for the  
Period January to December 1979", UKNDC(80)P96 NEANDC(E)  
212, Vol. 8, INDC (UK) - 32/LN, p. 22 United Kingdom Atomic  
Energy Authority, Harwell 1980.
20. F.H. FRÖHNER, "SESH - A FORTRAN IV Code for Calculating the  
Self-Shielding and Multiple Scattering Effects for Neutron  
Cross Section Data Interpretation in the Unresolved  
Resonance Region, "GA-8380, Gulf General Atomic Company  
(1968).
21. E. STORM and H.I. ISRAEL, Nucl. Data Tables A7, 565 (1970).
22. W.R. DIXON, Nucleonics 8, 69 (1951).
23. F.H. FRÖHNER, "FANAC - A Shape Analysis Program for Reso-  
nance Parameter Extraction from Neutron Capture Data for  
Light and Medium-Weight Nuclei", KfK 2145, Kernforschungs-  
zentrum Karlsruhe, 1977.
24. F.H. FRÖHNER, KEDAK-3 evaluation (1977), Data available  
on request from KfK Karlsruhe.

25. F.H. FRÖHNER, K. WISSHAK and F. KÄPPELER, "Recent Work on Structural-Material Cross Sections at Kernforschungszentrum Karlsruhe", KfK 2899, Kernforschungszentrum Karlsruhe, 1979.
26. G. ROHR, Proc. of the NEANDC/NEACRP Specialists Meeting on Fast Neutron Capture Cross Sections, Argonne, 20-23 April, 1982, to be published.
27. G. REFFO, private communications.
28. K. WISSHAK and F. KÄPPELER, Nucl. Sci. Eng. 77, 58 (1981).
29. K. WISSHAK, F. KÄPPELER, G. REFFO and F. FABBRI, Proc. of a Specialists Meeting on Fast Neutron Capture 20-23 April 1982, Argonne National Laboratory, Argonne, Ill., to be published.
30. B.J. ALLEN, D.D. COHEN, and F.Z. COMOANY, J. Phys. G. Nucl. Phys. 6, 1173 (1980).
31. F.G. PEREY, G.T. CHAPMAN, W.E. KINNEY and C.M. PEREY, Proc. Specialists' Meeting Neutron Data of Structural Materials for Fast Reactors, Geel, Belgium, December 5-8, 1977, p. 530, Pergamon Press, Oxford (1979).
32. S. IIJIMA and H. YAMAKOSHI, J. Nucl. Sci. Technol. 17, 477 (1980).
33. H.T. LIOU, R.E. CHRIEN, R.C. BLOCK, and U.N. SINGTH, Nucl. Sci. Eng. 70, 150 (1979).
34. B.J. ALLEN, J.W. BOLDEMAN, and R.L. MACKLIN, Nucl. Sci. Eng. 82, 230 (1982).
35. B.J. ALLEN, private communications.
36. H. BEER, L.D. HONG, and F. KÄPPELER, Nucl. Sci. Eng. 67, 184 (1978).
37. J.B. GARG, S. JAIN, and J.A. HARVEY, Phys. Rev. C18, 1141 (1978).
38. K. WISSHAK and F. KÄPPELER, Nucl. Sci. Eng. 66, 363 (1978).
39. G. REFFO, F. FABBRI, K. WISSHAK and F. KÄPPELER, Nucl. Sci. Eng. 80, 630 (1982).
40. P.A. SEEGER, W.A. FOWLER, and D.D. CLAYTON, Ap. J. Suppl. 11, 121 (1965).
41. D.D. CLAYTON, W.A. FOWLER, T.E. HULL, and B.A. ZIMMERMAN, Annals. Phys. 12, 331 (1961).

42. B.J. ALLEN, R.L. MACKLIN, and J.H. GIBBONS,  
Adv. Nucl. Phys. 4, 205 (1971).

TABLE I Parameters of the Neutron Source

Accelerator:	3 MV Van de Graaff
Proton energy:	20 keV or 135keV above ${}^7\text{Li}(p,n)$ threshold at 1.881 MeV
Repetition rate:	1 MHz
Pulse width:	700 ps
Beam intensity:	5 $\mu\text{A}$
Neutron beam:	white spectrum 10 to 80 keV or 5 to 250 keV
Target:	Water-cooled metallic lithium ( $\sim 1.8 \text{ mg/cm}^2$ ) on 0.3 mm thick tantalum backing
Flight path:	60.89 cm
Total time resolution:	1.2 ns
Energy resolution:	2 ns/m

TABLE II Compilation of the Relevant Sample Data <sup>a</sup>

Sample	Chemical Composition	Isotopic Composition	Weight (g)	Thickness (atom/b)
<sup>56</sup> Fe	metal	natural	9.901	$8.495 \times 10^{-3}$
<sup>58</sup> Fe	Fe <sub>2</sub> O <sub>3</sub>	1.14 % <sup>54</sup> Fe 1.86 % <sup>57</sup> Fe 23.74 % <sup>56</sup> Fe 73.26 % <sup>58</sup> Fe	19.619	$1.155 \times 10^{-2}$
<sup>197</sup> Au	metal	natural	23.525	$5.722 \times 10^{-3}$
C	graphite	natural	15.034	$5.997 \times 10^{-2}$

a. The diameter of all samples was 40 mm.

TABLE III Correction Factors for Multiple Scattering (MS) and Self-Shielding (SS) in the Gold Sample

Neutron Energy (keV)	MS x SS	Uncertainty (%)
5	0.994	1.0
10	1.046	1.0
20	1.075	0.9
40	1.075	0.8
80	1.069	0.7
160	1.065	0.8
320	1.047	0.6

TABLE IV Values taken as fixed parameters in the FANAC fits.

Isotope	s-Wave Strength Function $\times 10^{-4}$	s-Wave Radius (fm)	p-Wave Radius (fm)
$^{54}\text{Fe}$	7.6	4.6	5.3
$^{56}\text{Fe}$	2.5	6.1	5.4
$^{57}\text{Fe}$	4.3	5.5	5.4
$^{58}\text{Fe}$	4.3	6.1	5.4

TABLE V Resonance Parameters for Resonances in  $^{56}\text{Fe}$

Resonance Energy (keV)	$g\Gamma_\gamma \Gamma_n/\Gamma$ (eV)	Statistical Uncertainty (%)	Systematic Uncertainty (%)	Total Uncertainty (%)	$R = \frac{\text{Coincidences}}{\text{Anticoincidences}}$ (rel. units)
22.8	0.178	6.4	6.4	9.0	0.41
27.8	$\Gamma_\gamma = 1.043$ $\Gamma_n^\gamma = 1.45 \text{ keV}$	4.8	6.4	8.0	0.44
34.2	0.598	3.0	6.6	7.2	0.24
36.7	0.257	6.2	5.0	8.0	0.42
38.4	0.359	5.1	5.1	7.2	0.28
46.0	0.456	4.4	4.9	6.6	0.41
52.1	0.724	3.8	6.5	7.5	0.27
53.5	0.378	6.3	6.1	8.8	0.60
59.2	0.841	3.6	5.6	6.7	0.28
63.4	0.536	4.8	5.8	7.5	0.85
72.9 <sup>a</sup>	0.606	7.5	5.7	9.4	0.12
73.9 <sup>a</sup>	$\Gamma_\gamma = 0.862$ $\Gamma_n^\gamma = 0.53 \text{ keV}$ <sup>b</sup>	7.0	5.4	8.8	0.14
77.0	0.294	13.7	6.5	15.1	0.39
80.8	1.808	2.7	5.4	7.3	0.42
83.5	$\Gamma_\gamma = 0.537$ $\Gamma_n^\gamma = 1.05 \text{ keV}$ <sup>b</sup>	12.8	10.8	16.8	0.65
90.3	0.847	5.8	6.4	8.6	0.54
92.6 <sup>a</sup>	1.73	3.3	4.9	5.9	0.36
96.2 <sup>a</sup>	} 2.27	10.0	4.7	11.0	0.54
96.5 <sup>a</sup>					
102.7	1.48	4.2	4.6	6.2	0.39
105.8	1.57	4.1	5.2	6.6	0.12
112.6	1.09	6.0	5.4	8.1	0.27

a. Unresolved doublets

b. from Ref. 23

TABLE VI

Resonance Parameters for Resonances in  $^{58}\text{Fe}$ 

Resonance Energy (keV)	$g\Gamma_\gamma \Gamma_n/\Gamma$ (eV)	Statistical Uncertainty (%)	Systematic Uncertainty (%)	Total Uncertainty (%)	$R = \frac{\text{Coincidences}}{\text{Anticoincidenc.}}$ (rel. units)
10.4	$\Gamma = 0.797$ $\Gamma_n^Y = 0.27$ keV	4.8	10.7	11.7	0.37
19.3	0.239	3.8	9.4	10.1	0.83
26.1	0.191	4.7	7.1	8.5	0.68
29.3	0.177	5.4	8.6	10.1	0.48
34.6	0.296	3.9	10.2	10.9	0.82
37.6	0.250	4.5	5.1	6.8	0.72
41.9	0.414	3.8	5.4	6.6	1.04
43.3	$\Gamma = 1.20$ $\Gamma_n^Y = 4.9$ keV	4.0	7.7	8.7	0.52
45.8	0.569	3.5	6.4	7.3	0.41
53.5	0.054	26.7	39.2	47.4	-
54.5	0.313	5.7	6.5	8.6	0.63
61.7	0.473	6.0	5.2	7.9	0.59
66.7	$\Gamma = 0.436$ $\Gamma_n^Y = 0.83$ keV	12.8	7.0	14.6	0.61
68.5	0.734	3.2	5.0	5.9	0.94
73.7	0.733	4.6	6.5	8.0	0.34
79.2	0.274	12.8	27.1	30.0	-
86.1	0.507	8.5	8.3	11.9	0.64
88.8	1.157	4.5	6.1	7.6	0.60
92.5	0.795	8.8	8.1	12.0	-
93.0	$\Gamma = 1.0$ $\Gamma_n^Y = 8.0$ a			~20	-
97.9	0.738	22.2	16.8	27.8	-

a from Ref. 12

TABLE VII

Systematic Uncertainties<sup>a</sup> of Resonances in <sup>56</sup>Fe

Resonance Energy (keV)	Background Gold Spectrum (%)	Background Iron Spectrum (%)	Weighting Function (%)	Structure in Gold Cross Section (%)	Isotopic Impurities (%)
22.8	1.0	2.0	0.7	3.6	1.8
27.8	0.7	4.0	2.1	0.7	0.5
34.2	1.0	0.7	1.1	4.7	-
36.7	1.0	2.0	0.4	0.9	-
38.4	1.0	1.6	0.5	0.3	1.7
46.0	0.7	1.5	0.9	1.2	-
52.1	0.4	1.4	1.5	4.3	0.5
53.5	0.4	2.2	1.6	2.7	1.6
59.2	0.4	1.3	2.1	2.4	0.6
63.4	0.4	1.5	1.2	3.2	-
72.9	0.4	1.0	1.5	3.1	0.3
73.9	0.4	2.0	1.6	1.8	-
77.0	0.4	2.9	1.6	2.4	2.3
80.8	0.4	1.1	0.9	2.8	0.2
83.5	0.4	3.6	0.5	8.9	2.2
90.3	0.4	2.0	0.3	4.2	-
92.6	0.4	0.5	0.9	1.9	-
96.2	0.4	1.5	0.5	1.5	0.2
96.5	0.4	0.3	0.5	1.2	0.2
102.7	0.4	1.0	0.2	0.5	0.2
105.8	0.4	1.4	0.7	2.3	0.2
112.6	0.4	2.3	1.0	1.5	0.9

a. In order to get the total systematic uncertainty a value of 4.4 % to all resonances has to be added according to Table IX

TABLE VIII Systematic Uncertainties <sup>a</sup> of Resonances in <sup>58</sup>Fe

Resonance Energy (keV)	Background Gold Spectrum (%)	Background Iron Spectrum (%)	Weighting Function (%)	Structure in Gold Cross Section (%)	Isotopic Impurities (%)
10.4	2.3	6.5	0.5	6.8	-
19.3	0.9	1.6	0.4	8.1	-
26.1	0.6	2.7	1.2	4.7	-
29.3	0.5	6.7	1.0	2.8	-
34.6	0.4	3.7	0.8	3.7	7.6
37.6	0.4	1.4	0.2	2.1	-
41.9	0.3	2.5	0.1	1.9	0.3
43.3	0.3	5.6	0.1	3.0	-
45.8	0.2	2.0	0.7	2.9	2.9
53.5	0.2	3.5	0.7	8.0	38.
54.5	0.2	3.5	0.3	3.1	1.0
61.7	0.2	2.3	0.5	1.6	0.3
66.7	0.2	4.5	0.5	2.9	0.5
68.5	0.2	1.7	0.2	1.6	0.3
73.7	0.2	1.3	0.8	3.1	3.4
79.2	0.2	2.8	0.4	1.9	26.5
86.1	0.2	2.7	0.5	6.4	0.8
88.8	0.2	1.2	0.5	3.7	1.4
92.5	0.2	1.5	0.6	5.6	3.4
97.9	0.2	4.2	0.4	11.0	11.1

a. In order to get the total systematic uncertainty a value of 4.4 % common to all resonances has to be added according to Table IX.

TABLE IX Systematic Uncertainties Common to All Resonances

Gold capture cross section:	2.5 %
Gamma-ray self absorption:	1.4 %
Multiple scattering and self shielding:	1.0 %
Pile-up events:	2. %
Threshold in gamma detector:	1. %
Neutron flux:	1. %
Fanac fit:	2. %
<hr/> Total	<hr/> 4.4 %

TABLE X Maxwellian Average Cross Sections for Various Thermal Energies

Thermal Energy (keV)	<σv> (mb)	
	<sup>56</sup> Fe	<sup>58</sup> Fe
20	13.9	16.5
25	14.0	15.1
30	13.9 ± 1.1	14.3 ± 1.4
35	13.7	13.7
40	13.5	13.3

FIGURE CAPTIONS

- Fig. 1 Schematic view of the experimental set-up.
- Fig. 2 Weighted TOF spectra of the four samples used in the measurement on  $^{56}\text{Fe}$  (energy range 5-250 keV). The peak around channel 960 is the prompt gamma-ray peak. The peak around channel 200 is caused by a satellite pulse.
- Fig. 3 Weighted TOF spectra of the four samples taken in one of the measurements on  $^{58}\text{Fe}$  (energy range 5-80 keV).
- Fig. 4 Various steps of background subtraction in the  $^{56}\text{Fe}$  measurement.
- Fig. 5 Various steps of background subtraction in the  $^{58}\text{Fe}$  measurement (same run as displayed in Fig. 3).
- Fig. 6 The three different methods applied for normalization to the gold standard. The solid line in the gold spectra is the counting rate used in the evaluation in conjunction with the respective standard cross section.
- Fig. 7 FANAC fit to the capture yield of  $^{56}\text{Fe}$ . The dashed line is the background due to isotopic impurities.
- Fig. 8 FANAC fit to the capture yield of  $^{58}\text{Fe}$  (all four runs added). The dashed line is the background due to isotopic impurities and due to capture of neutrons scattered in the 43.3 keV resonance (see text).
- Fig. 9 FANAC fit to the capture yield of  $^{56}\text{Fe}$  as obtained from the unweighted coincidence spectra.
- Fig. 10 FANAC fit to the capture yield of  $^{58}\text{Fe}$  as obtained from the unweighted coincidence spectra.

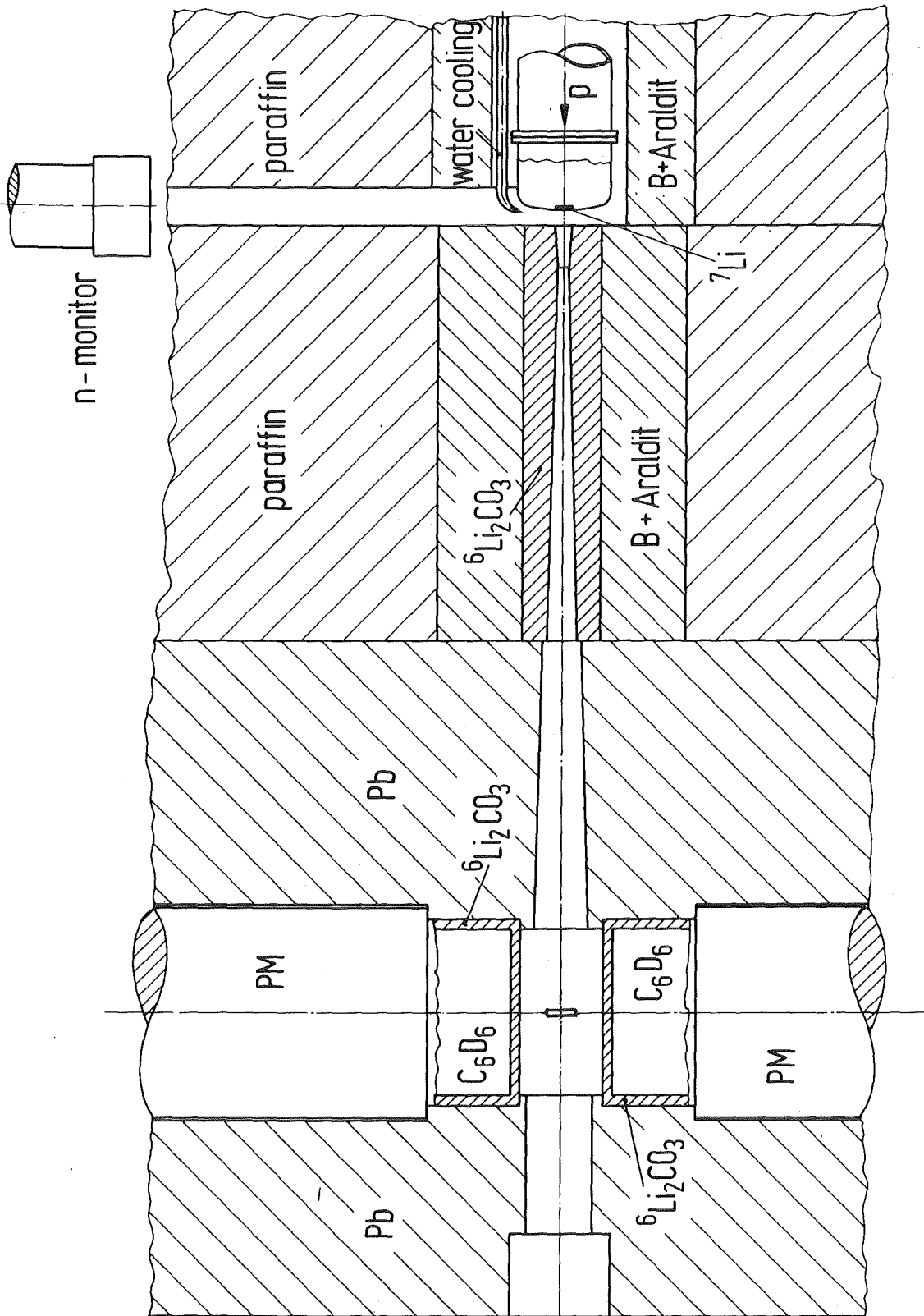


Fig. 1

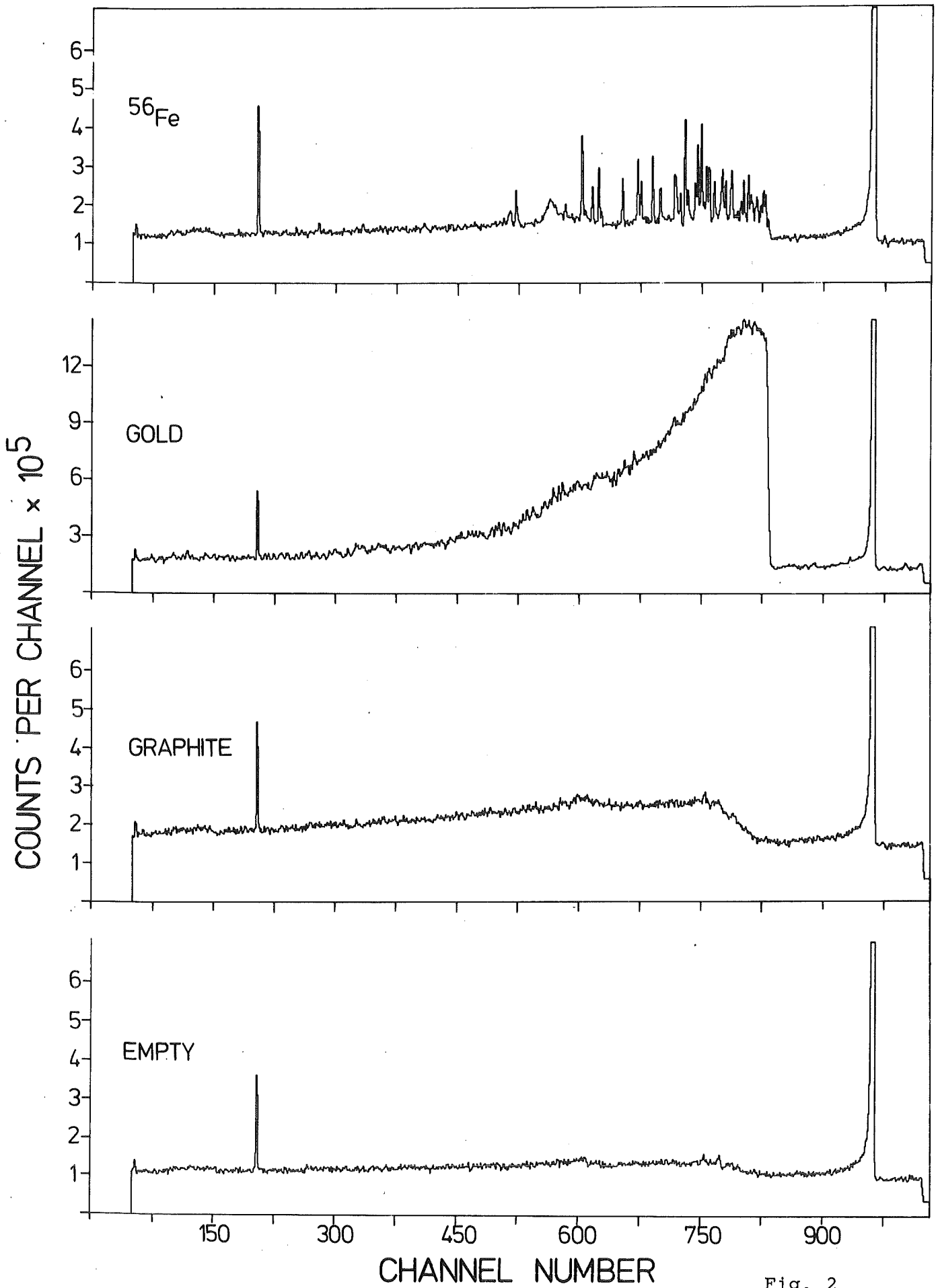


Fig. 2

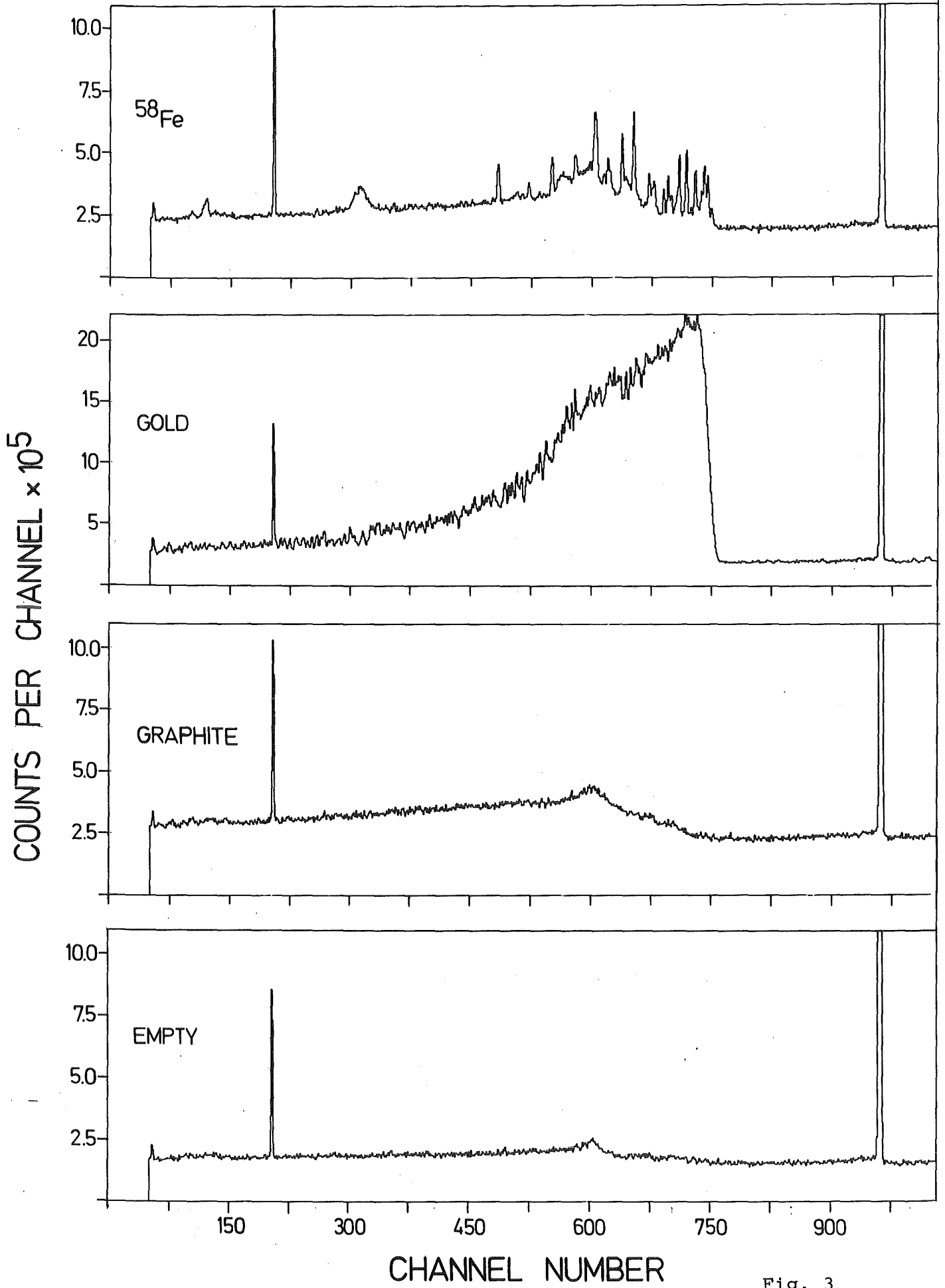


Fig. 3

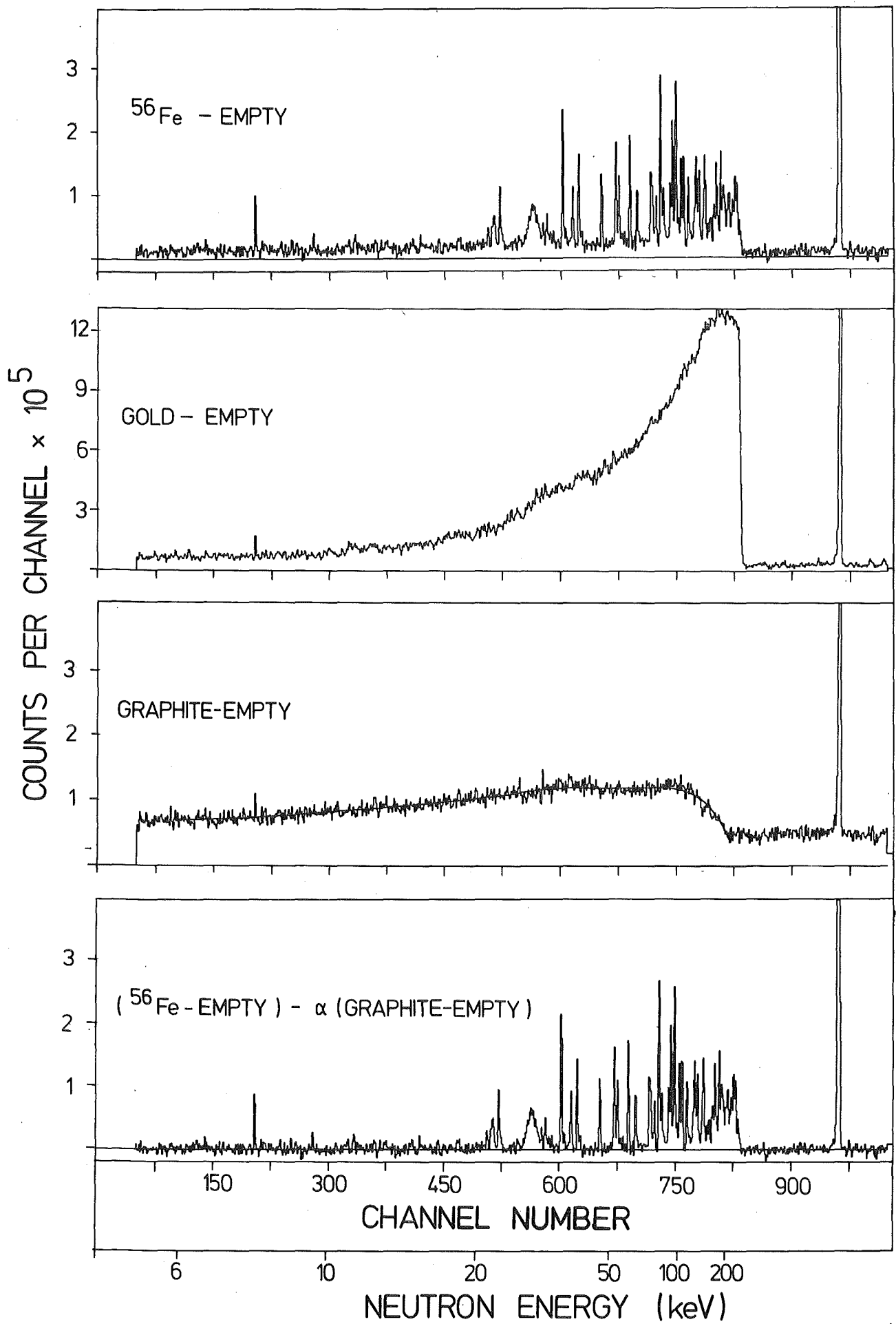


Fig. 4

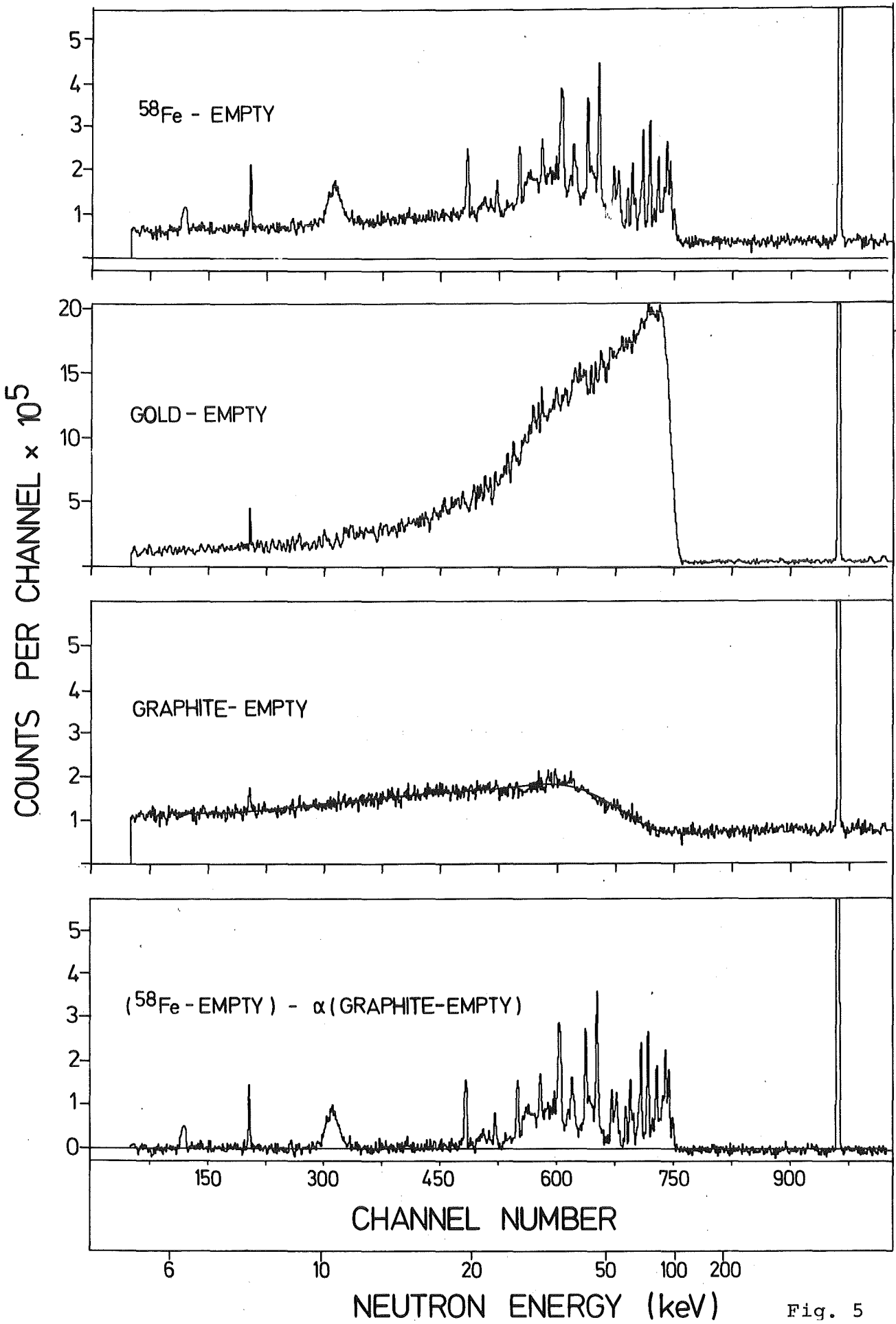


Fig. 5

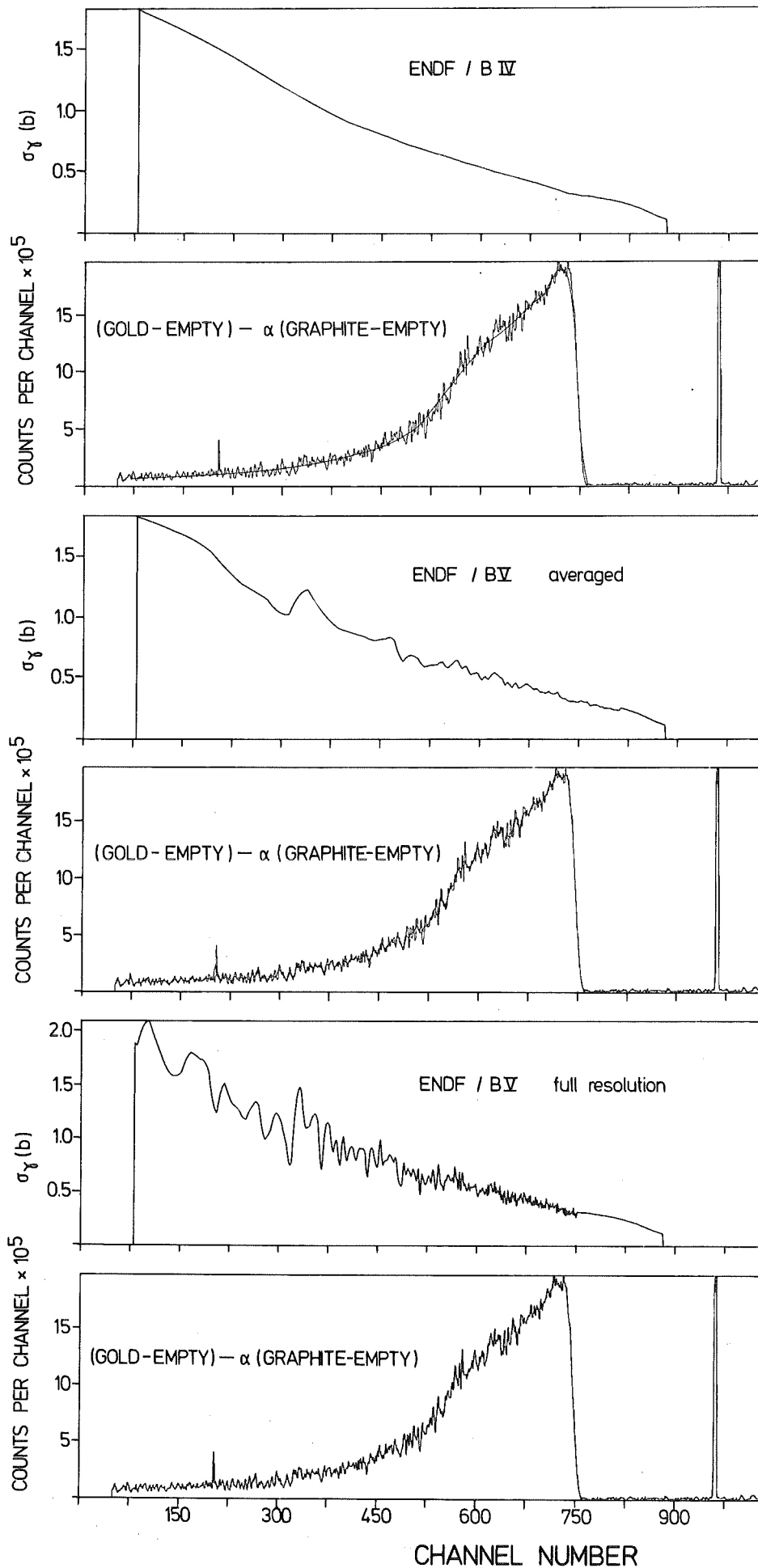


Fig. 6

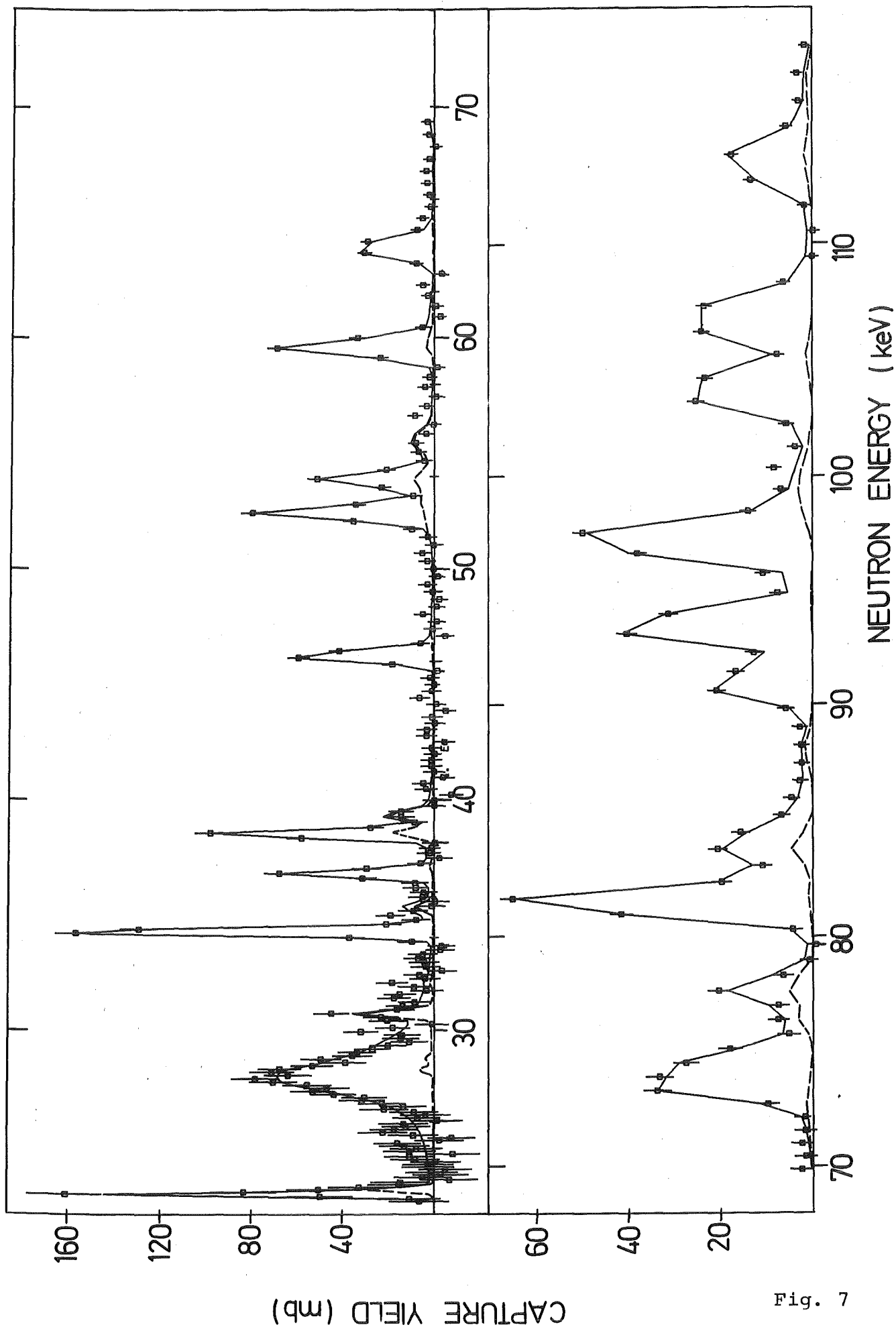


Fig. 7

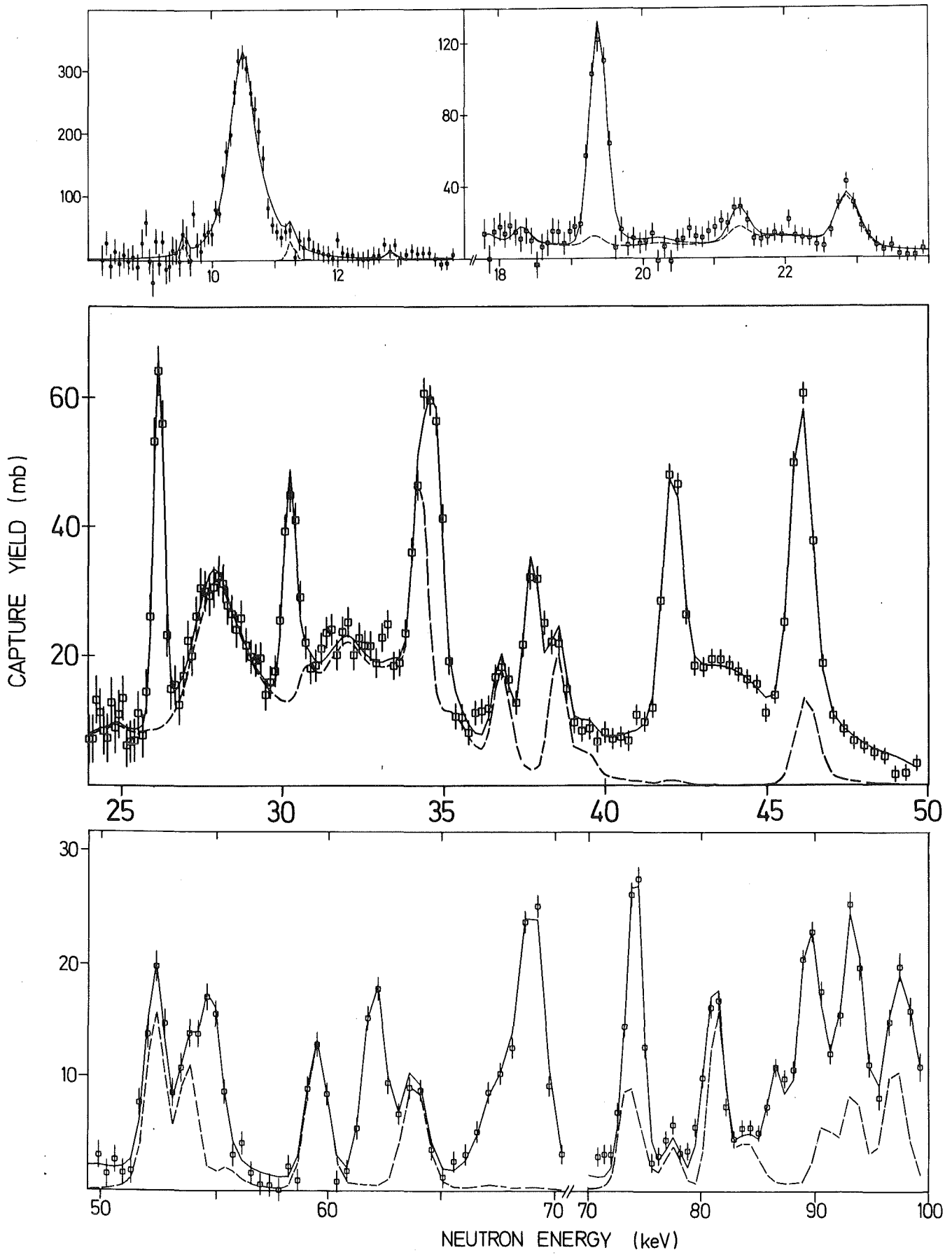


Fig. 8

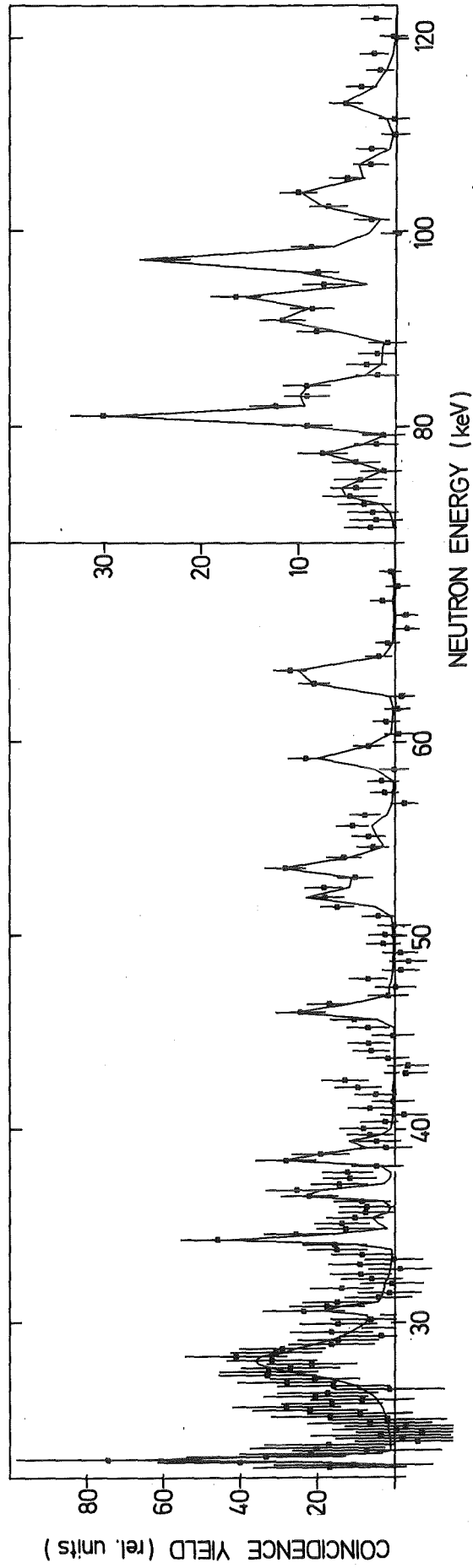


Fig. 9

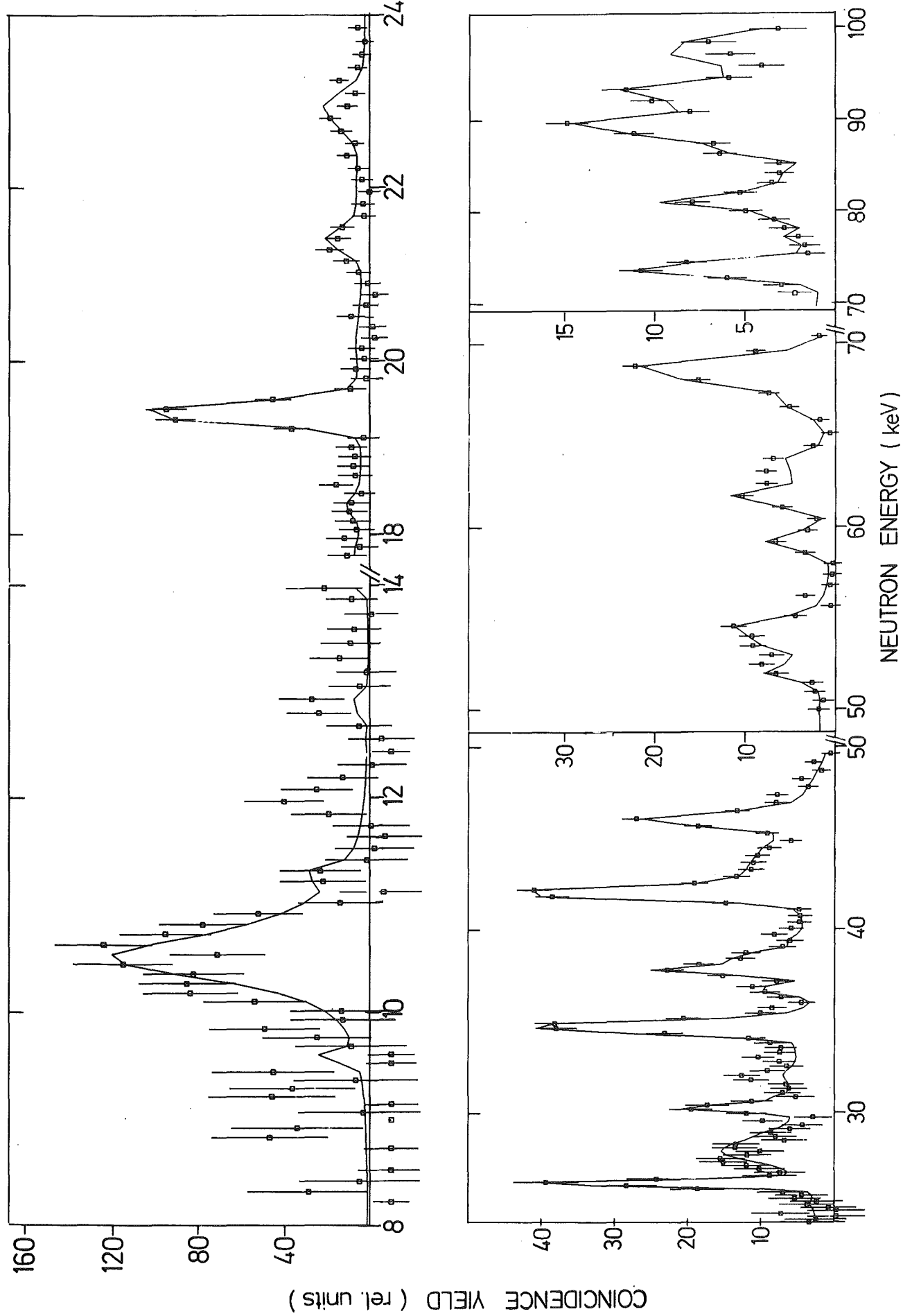


Fig. 10